International Journal of Heat and Mass Transfer 52 (2009) 1337–1352

Contents lists available at ScienceDirect

International Journal of Heat and Mass Transfer

journal homepage: www.elsevier.com/locate/ijhmt

Fluid flow and convective heat transfer in flat microchannels

Omar Mokrani, Brahim Bourouga, Cathy Castelain, Hassan Peerhossaini *

Thermofluids, Complex Flows and Energy Research Group, Laboratoire de Thermocinétique de Nantes, UMR-CNRS 6607, Ecole polytechnique de l'université de Nantes, BP 50609, 44306 Nantes Cedex 3, France

ARTICLE INFO

Article history:
Received 23 November 2007
Received in revised form 30 July 2008
Available online 29 October 2008

Keywords:
Rectangular microchannels
Microfluidics
Micro-convection
Inverse method
Nusselt number
Experimental study

ABSTRACT

This study investigates the design, construction and instrumentation of an experimental microchannel, with a rectangular cross-section and large aspect ratio, that allows characterization of the flow and convective heat transfer under well defined and precise conditions and makes it possible to vary the hydraulic diameter of the microchannel. The flow friction coefficient is estimated by direct pressure drop measurements inside the microchannel in a zone where the flow is fully developed. Since the wall thermal conditions inside the microchannel can not be measured directly, their estimation requires temperature measurements in the wall thickness and an inverse heat conduction method. The thermal and hydrodynamic results obtained by varying the hydraulic diameter between 1 mm and 100 μm do not deviate from the theory or empirical correlations for large-scale channels. These results let us confirm that for smooth walls the continuum mechanics laws for convection and fluid mechanics remain valid in microchannels of hydraulic diameter greater than or equal to 100 μm.

1. Introduction

Straight channel flow and convective heat transfer in channel flow are frequently considered fully understood. However, progress over the last decade in miniaturization of various technological devices has led to the new discipline of microfluidics, which regroups various scientific domains concerning flows in structures or devices of length scales from one to a few hundred microns. Many studies have recently been dedicated to characterizing the heat transfer in microchannels in components of electronic cooling applications. The results of various workers show a broad dispersion of experimentally determined Poiseuille numbers and convective heat transfer coefficients (Figs. 1 and 2). Indeed, some studies revealed an increase in convective heat transfer with reduction in the hydraulic diameter for different channel geometries (Choi et al., 1991 [1]; Rahman and Gui, 1993 [2]; Yu et al., 1995 [3]; Cuta et al., 1996 [4]; Adams et al., 1998 [5]; Rahman, 2000 [6]). On the other hand, other work revealed a decrease in convective heat transfer with channel size compared to the 'large-scale' channels (Peng and Wang, 1993 [7]; Wang and Peng, 1994 [8]; Tso and Mahulikar, 2000 [9]; Qu et al., 2000 [10]; Debray et al., 2001 [11]; Gao et al., 2002 [12]). Finally, some experimental studies reveal no sensitivity of the convective heat transfer coefficient to the channel hydraulic diameter (Qu and Mudawar, 2002 [13]; Lelea et al., 2004 [14]; Lee et al., 2005 [15]).

Many reasons have been suggested to explain the deviation from classical theory. The high relative wall roughness coupled with its nonuniformity could generate a large hydraulic diameter, as mentioned by Pfahler et al., 1991 [16]. The same authors suggested that the deviations could be due to the reduction in the apparent viscosity of the fluid with the reduction in hydraulic diameter. Another hypothesis in the literature suggests that the momentum transfer increase could be caused by roughness in the wall boundary layers. Mala and Li (1999) [17] showed the influence of roughness by introducing a viscosity model that depends on channel roughness μ_R (roughness-viscosity). This model originates in the work of Merkle et al. (1974) [18] and Tani (1969) [19], who showed that the presence of roughness affects the flow velocity profile and the transitional Reynolds number. A third hypothesis put forward and modelled by Mala et al. (1997) [20] assumes that the observed deviations from the classical laws in the microchannels are due to the interactions between the electric charge of the fluid and that of the wall, a double electric layer resulting from the imbalance between the fluxes of cations and anions. The influence of the double electric layer on the velocity profiles and friction coefficients is small compared to the Poiseuille flow, less than a few hundred percent (Colin, 2004) [21], and its influence on convective heat transfer decreases with the ratio of channel height to double electric layer thickness. Most of the work in the literature (Peng et al., 1995 [22]; Wang and Peng, 1994 [8]; Rahman, 2000 [6]) was carried out under experimental conditions in which this ratio is high.

The fourth hypothesis in the literature to explain the reduction in the pressure losses and convective heat transfer with channel diameter reduction was suggested by Sabry (2000) [23]: that a layer of air remains trapped between the fluid and the wall all along the channel. This air layer thermally isolates the wall from

* Corresponding author. Tel.: +33 2 40 68 31 24; fax: +33 2 40 68 31 41.
E-mail address: hassan.peerhossaini@univ-nantes.fr (H. Peerhossaini).

0017-9310/$ - see front matter © 2008 Elsevier Ltd. All rights reserved.
doi:10.1016/j.ijheatmasstransfer.2008.08.022

Nomenclature

a	plate thickness, m
b	plate width, m
b'	thickness of the uniform temperature zone, m
C	heat transfer coefficient parameter
C^o	heat transfer coefficient parameter at initial iteration
C_p	heat capacity, J kg^{-1} K^{-1}
e	microchannel height, m
f	friction coefficient
$h(x)$	local heat transfer coefficient, W m^{-2} K^{-1}
h_∞^0	fully developed heat transfer coefficient at initial iteration, W m^{-2} K^{-1}
h_∞	fully developed heat transfer coefficient, W m^{-2} K^{-1}
$J(\delta_k)$	least-squares function, K^2
k_f	fluid thermal conductivity, W m^{-1} K^{-1}
k_s	solid thermal conductivity, W m^{-1} K^{-1}
L	microchannel length, m
N_t	number of thermocouples
Nu	local Nusselt number
Nu_{exp}	experimental Nusselt number
Nu_m	average Nusselt number
Nu_{th}	theoretical Nusselt number
Po	Poiseuille number
Po_{exp}	experimental Poiseuille number
Po_{th}	theoretical Poiseuille number
q''	volume heat generation, W m^{-3}
q	heat flux density, W m^{-2}
Re	Reynolds number
S_c	sensitivity of parameter C in solid, K m^{-1}
S_h	sensitivity of parameter h_∞ in solid, K^2 m^2 W^{-1}
S_c^f	sensitivity of parameter C in fluid, K m^{-1}
S_h^f	sensitivity of parameter h_∞ in fluid, K^2 m^2 W^{-1}
T	temperature, K
T_f	bulk fluid temperature, K
T_{in}	fluid inlet temperature, K
T_{out}	fluid outlet temperature, K
T_p	wall temperature, K
$\tilde{T}_i(\delta_k)$	temperature calculated numerically at iteration k, K
T_i^*	temperature measured experimentally, K
T_p	wall temperature
U	mean velocity, m s^{-1}
x, y, z	Cartesian coordinates
X^*	Cameron number

Greek symbols

α	relaxation coefficient
α^*	aspect ratio
β	relaxation coefficient
ε	convergence criterion
ρ	density, kg m^{-3}
δ^k	displacement vector
μ^k	under-relaxation coefficient
μ^R	roughness-viscosity

the fluid and leads to a reduction in convective heat transfer and hence to the reduction of the Nusselt numbers observed in some studies.

In addition, the ability of the Navier–Stokes and energy equations to represent the flow and heat transfer behavior adequately in microchannels is called into question in some of these studies. If, however, the explanations and models suggested by several authors are convincing only for channel hydraulic diameters of a few microns or nanometers, they do not explain the deviations observed in some studies with channel hydraulic diameters of the order of millimeters, much less the dispersion of the results. In a recent review article Guo and Li 2002 [24] and Hetsroni et al. 2005 [25] reported the dominant factors and phenomena in the flow and heat transfer as the device scale decreases.

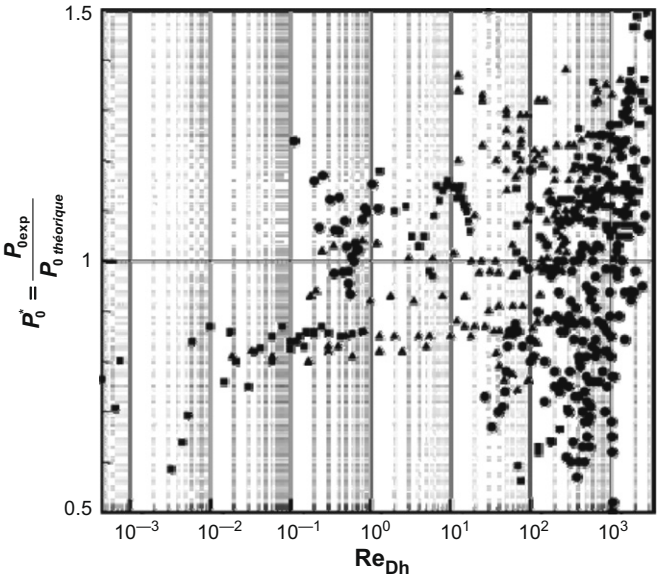

Fig. 1. Poiseuille number determined experimentally. ■ Pfahler et al. [40], Pfund et al. [38], Papautsky et al. [39]; ▲ Pfahler et al. [16], Wilding et al. [41], Qu et al. [10], Flockart et al. [43]; ● Choi et al. [1], Jiang et al. [42], Mala et al. [17], Judy et al. [37].

One of the main causes of this dispersion can be measurement errors and errors in estimating the parameters governing the convective heat transfer coefficient. Indeed, in most experiments, flows are in the entrance developing zone, and because of the axial variation of the convective heat transfer coefficient the heat flux lines are greatly deformed in the wall's thickness. Some studies have compared Nusselt and Poiseuille numbers estimated for thermally or hydrodynamically undeveloped flows with the Nusselt and Poiseuille numbers of fully developed flows. In addition to measurement errors, which can be significant, the use of one-dimensional models to describe heat transfer in the microchannel walls can cause considerable error.

The aim of this study is to develop a reliable experimental device and adequate methodology to characterize the flow and convective heat transfer in flat microchannels. It is organized as follows: Section 2 describes the experimental apparatus and methods used here, the design considerations for the flat microchannel, and its instrumentation. Section 3 presents the methodology for the simultaneous estimation of the wall thermal conditions and convective heat transfer coefficient. Finally, the experimental results on fluid flow and heat transfer in the microchannel are presented in Section 4 and conclusions are drawn in Section 5.

2. Experimental apparatus and methods

2.1. Water tunnel

A water tunnel facility was specially designed and constructed in order to provide a well controlled flow through the test section. The test facility, the open-loop water tunnel shown schematically in Fig. 3, was designed for the analysis and characterization of single-

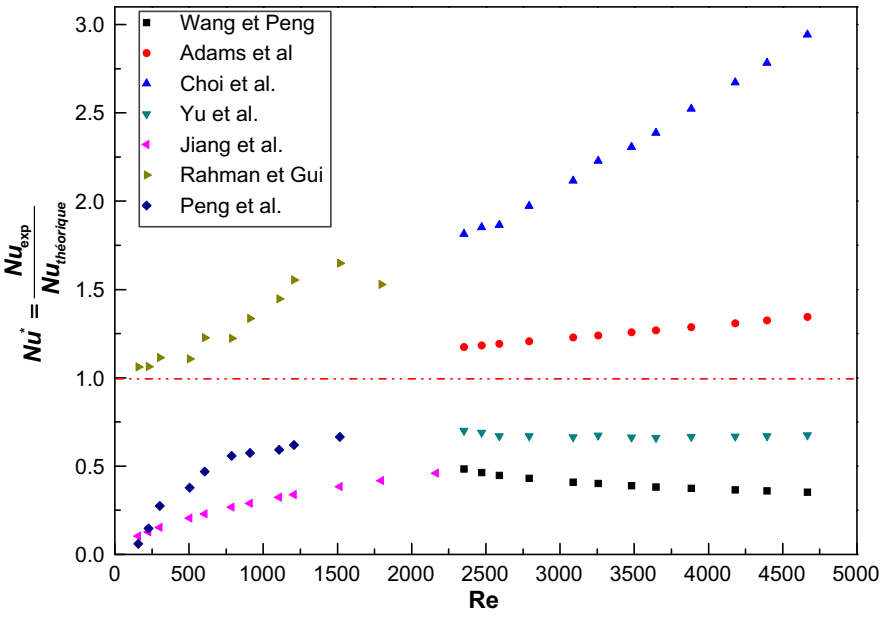

Fig. 2. Convective heat transfer determined experimentally.

phase flow and heat transfer inside a flat microchannel of high aspect ratio (width/height). The channel width is constant and its height is variable between 50 and 500 μm. The working fluid, tap water, flows in the test loop with an offset screw pump for flow rates ranging from 0.04 to 240 l/min, a range that allows the exploration of laminar, transitional and turbulent flow regimes ($100 < Re < 5000$). The working fluid temperature at the microchannel inlet is kept constant during the experiments. 0.1 μm filters fixed upstream of the microchannel prevent the entry of solid particles, and an upstream damping pipe absorbs possible vibrations generated by the pump.

The mass flow rate was determined by weighing the working fluid leaving the microchannel using a 0.1 g precision digital balance.

2.2. Microchannel

The microchannel, shown schematically in Fig. 3, is a straight microchannel of rectangular cross-section of high aspect (width to height) ratio and is made by superposing two parallel stainless steel plates of thickness a, width b, and heated length *L*. Two stainless steel foils separate the plates and complete the channel as shown in Fig. 3. They constitute the lateral walls of the channel and determine its height *e*. The parallel plates are made of several instrumented stainless steel blocks of various thicknesses stuck together. In order to avoid heat losses in the channel entrance and exit, 3 mm Plexiglas blocks are placed in front of and at the end of the stainless steel blocks for insulation for accurate control of the heated zone of the microchannel. To avoid flow perturbation, convergent and development lengths are added before and after the Plexiglas blocks at the channel entrance and exit. The convergent length reduces the effect of the abrupt contraction singularities at the entrance and exit of the microchannel; the development length allows the relaxation of the flow streamlines and the development of a Poiseuille flow. The relaxation length is 60 times the hydraulic diameter, ensuring fully developed Poiseuille flow at the microchannel entrance.

The pressure holes instrumented by piezoelectric sensors in the stabilization blocks allow pressure loss measurements upstream and downstream of the heating zone. Each of the different stainless steel blocks constituting the two parallel plates is instrumented by three K-type thermocouples of bead diameter 50 μm fixed in the slab thickness. Finally, the stainless steel blocks, the convergent length, the Plexiglas insulators, and the stabilization blocks that constitute the upper and the lower microchannel walls are glued together. Uniform flux heating is provided to the slabs through electric heating elements of 2 mm diameter introduced into the U-shaped grooves machined on the outer surface of each slab. A final operation of rectification, leveling, and smoothing is carried out on the inner surface of the slabs to guarantee perfect flatness and smoothness in the microchannel walls and to remove any singularity that could disturb the flow. In order to find the exact positions of the thermocouples, three-dimensional geometrical measurements are made on the inner faces of the blocks before and after rectification; moreover, the exact thermocouple positions can be checked at the end of the experiments by separating the blocks.

The microchannel is thermally isolated from its surroundings by Deltherm insulating panels. In addition, a natural rubber seal placed inside a groove machined on the upper and lower slabs ensures water-tightness between the slabs and the lateral walls. This insulation, in addition to that ensured by the Plexiglas, permits control of the heating zone and minimization of heat losses.

2.3. Microchannel design

One of the difficulties in the experimental study of microchannel heat transfer is the ambiguity in the channel thermal boundary conditions, in particular the uniformity of the solid wall heat fluxes and also the exact wall surface temperature. Wall surface temperature can be incorrect because of the interaction of the temperature probe with the wall materials: the presence of the probe can perturb the wall heat flux. Both design concepts and the microchannel wall dimensions must take into account this important criterion. Another source of error in evaluating the convective heat transfer coefficient is the hydrodynamic conditions of the microchannel flow: whether the flow is a fully developed Poiseuille flow or a developing flow affects the convective coefficient. In order to avoid these sources of error here we decided to work in fully developed channel flow conditions, and thus we verified this condition in designing the microchannel.

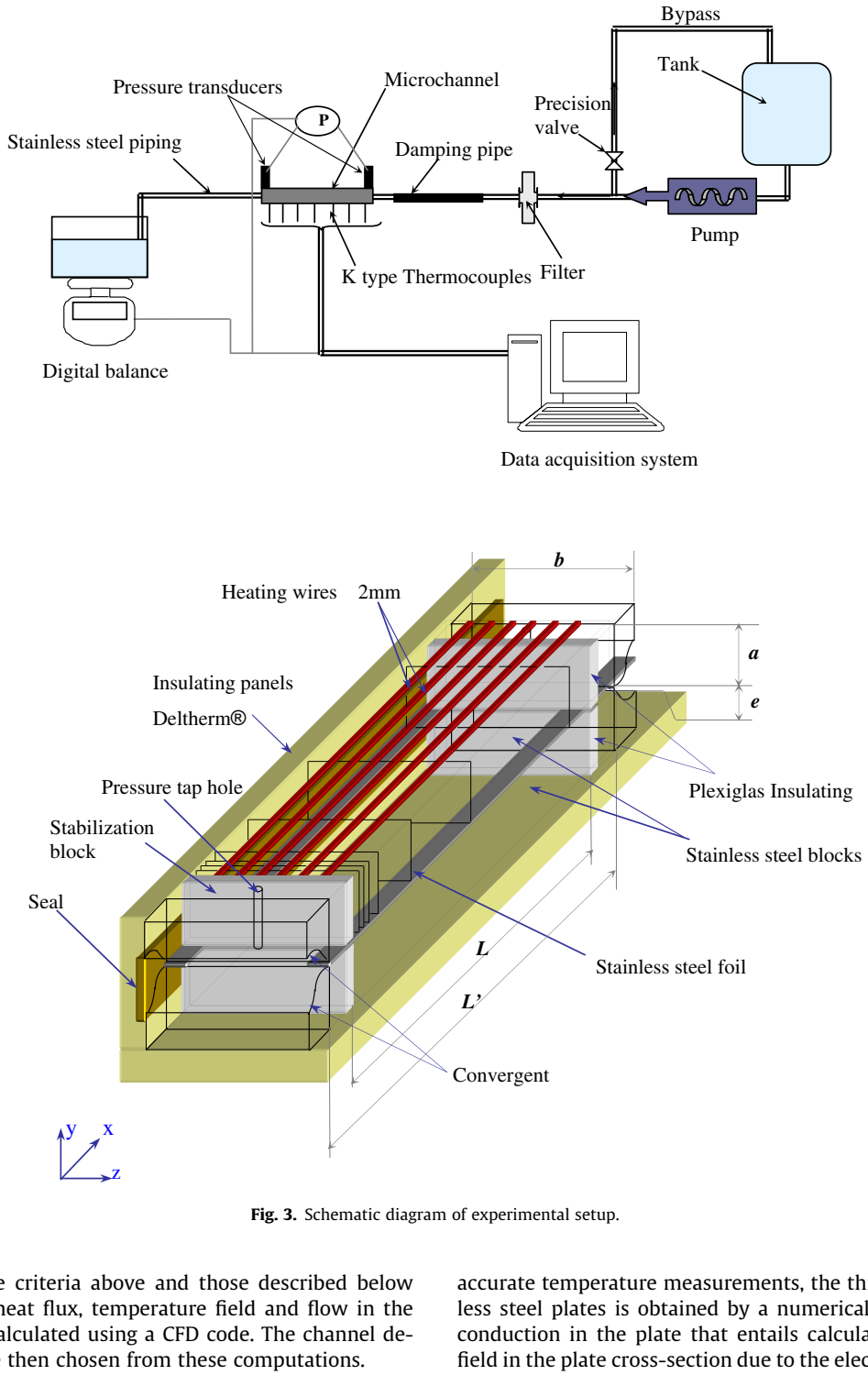

Fig. 3. Schematic diagram of experimental setup.

To assure that the criteria above and those described below were fully satisfied, heat flux, temperature field and flow in the microchannel were calculated using a CFD code. The channel design parameters were then chosen from these computations.

The channel height e determines the macro or micro character of the channel. This height is determined by the thickness of the metallic foils that separate the two parallel plates constituting the microchannel walls. Varying the thickness of the foils between 500 and 50 μm varies the channel height and hydraulic diameter between 1 mm and 100 μm.

The parallel plate's thickness *a* and width *b* are determined by searching for heat flux uniformity in the channel walls. The intrusion of the heating wire on the outside faces of the stainless steel plates includes a thermal macroconstriction that is propagated up to a certain depth where the temperature field is three-dimensional. In order to avoid the thermal constriction zone and achieve accurate temperature measurements, the thickness a of the stainless steel plates is obtained by a numerical computation of heat conduction in the plate that entails calculating the temperature field in the plate cross-section due to the electric power dissipation in the heating wires. Fig. 4, a schematic of the thermal model of the channel wall cross-section, describes the heat insulation on the outside surface of the plate by a zero heat flux. The bottom face is described by a condition of fluid convection inside the microchannel, and the convective heat transfer coefficient used is that in Shah and London's (1978) [26] correlations. Finally, the heating wires are modelled by a uniform heat source. The numerical isothermal lines in Fig. 4 show that the thickness of the zone thermally disturbed by the heating wires is approximately 10–15 mm. Thus taking the plate thickness larger than 20 mm ensures that we are in the parallel isothermal zone and hence can place the thermocouples correctly.

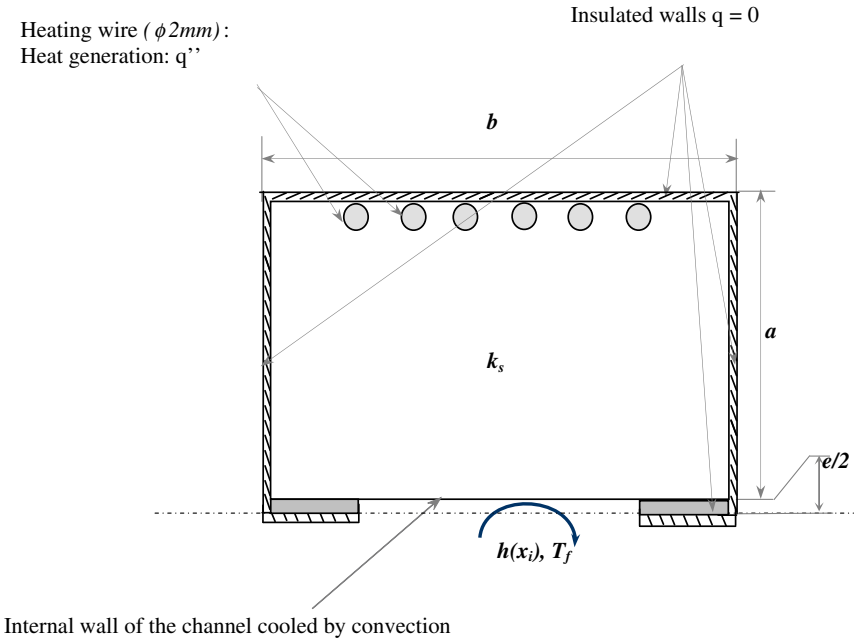

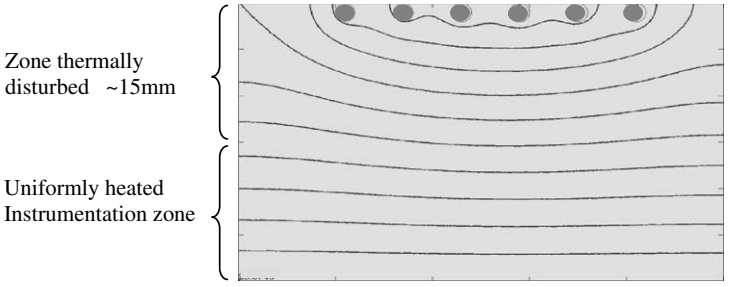

Fig. 4. Thermal model used in studying the heating system and influence of the heating system.

Note that the plate width b is important in both the solid and fluid zones of the system. Indeed, in the fluid part, the microchannel width determines the two-dimensionality of the flow; in the solid part, the plate width influences the temperature field uniformity in the instrumented wall zone. Note that the wall temperature at the fluid–solid interface is estimated from only one measurement located at the middle of the channel width. This temperature must consequently be uniform along the channel width for a given axial position in the channel. The channel aspect ratio (width/height) must be greater than 10 for the flow to be considered two-dimensional. In this study, a channel width b greater than approximately 10 mm is generally sufficient. Fig. 5a plots temperature distribution versus channel width for channel width b of 10 mm and plate width of 50 mm with the same boundary conditions as in the previous paragraph. This figure shows the notable effect of the macroconstriction on the temperature field, which makes the thermocouple instrumentation very delicate. Therefore, we opted for a channel width of 30 mm and plate width of 50 mm. These dimensions ensure on the one hand a uniform isothermal zone sufficiently large (see also Fig. 5b) to allow the thermocouples' "thermalisation" and thus avoid conduction effects in thermocouple wires. On the other hand, the temperature measurement in the wall center will be representative of the temperature all along the channel width, thus letting us use a two-dimensional model according to (x, y) for the system, the z direction being uniform.

Determination of the heating length L of the wall plates depends on the hydrodynamic and thermal development lengths. Indeed, the channel length must be sufficiently long to explore heat transfer at the entrance and in the fully developed zones. For the hydraulic diameters studied here, the hydrodynamic development length was estimated as 25 mm maximum for laminar regime. The stabilization blocks and the Plexiglas insulators fixed in the channel entry offer sufficient length for hydrodynamic development of all the flow regimes studied here. For the thermal development, two heated lengths were retained. The first, 297 mm, was used for channel heights above 100 μm. For channel heights of 100 and 50 μm, the channel heated length was reduced to 97 mm due to pump capacity limitations. Finally, the selected lengths allow the fluid flow and heat transfer study of both (hydrodynamically and thermally) fully developed and developing cases.

3. Estimation of the convective heat transfer coefficient in the microchannel

Estimation of the convective heat transfer inside channels requires knowledge of the convective heat transfer coefficient. The determination of its evolution along the microchannel requires knowledge of three parameters: the wall surface temperature, the wall heat flux density, and the bulk fluid temperature. The first two parameters being inaccessible to direct measurement, their

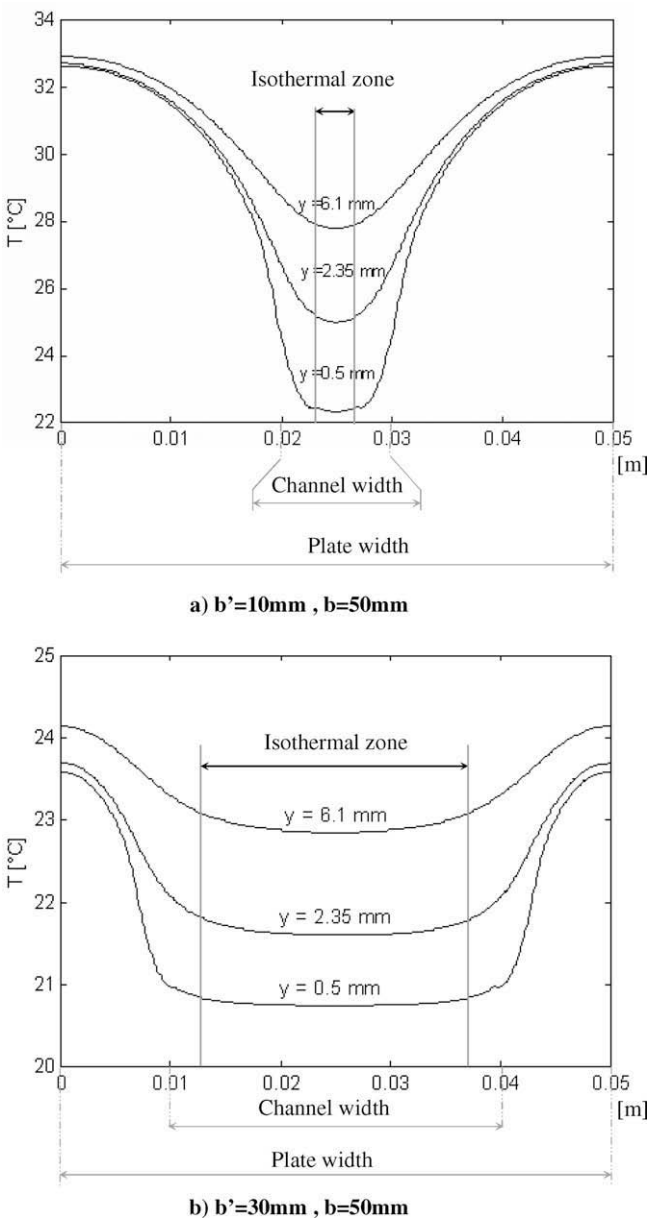

Fig. 5. Evolution of temperature distribution in channel width for various heights.

determination requires the use of an inverse method. This method requires on the one hand modelling of the phenomena present in the system and on the other the measurement of a certain number of temperatures at specific positions in the wall thickness. The evolution of the bulk fluid temperature along the channel can be obtained numerically using measurements of the inlet and the outlet fluid temperatures as boundary conditions.

The main parameter required in our study is the convective heat transfer coefficient characterizing the heat transfer between fluid and channel walls. Our estimation method requires a preliminary choice of the temperature evolution function. Since the flow is in the entrance-zone, the convective conductance was assumed to follow the Eq. (1). This expression, in fact, lets us take into account the axial evolution of the convective heat transfer in the thermal development zone. This consideration reduces determination of the convective heat transfer coefficient to the knowledge of two parameters, C and h_∞:

$$h(x) = h_\infty \cdot \left(1 + \frac{C}{x}\right) \tag{1}$$

The inverse method developed here requires knowledge of the temperature distribution and the sensitivities at the probe positions. The two parameters C and h_∞ can be determined by resolution of the direct and sensitivity problems, as described below.

3.1. Mathematical modelling of heat transfer in the microchannel

The quality of the estimates of the various parameters is directly related to the relevance of the mathematical model used in the inverse method to describe the heat transfer problem. This study is concerned with heat transfer by a Newtonian fluid flow inside a flat microchannel of rectangular cross-section whose aspect ratio is sufficiently high that the flow can be considered two-dimensional. In this case the hydraulic diameter is twice the channel height e. Fig. 6a shows a schematic diagram of the problem to be modeled; the two solid plates represent the microchannel walls and the fluid in the center represents the flow zone inside the microchannel.

The mathematical model used to describe the convective heat transfer between the walls and the fluid takes into account the whole field (solid wall and fluid layer) and the coupling between the conduction and the convection modes. The symmetry of the experimental device reduces the study to the half of the field, with boundary conditions as described in Fig. 6b. The solid part of the system is modelled by the equation of steady two-dimensional conduction (2a). By proceeding to an energy balance on the channel and using the bulk temperature, the fluid field can be modelled by a one-dimensional equation of convection-diffusion with a heat source term (2b). This choice of model allows determination of the convective conductance directly in the inverse problem. Indeed, since the convective heat transfer coefficient is defined with a bulk temperature, the resolution of the selected model directly determines the latter. The coupling between the two fields is translated in the model of the solid part by the boundary condition at the liquid–solid interface (2e) and in that of the fluid part by the source term.

$$\frac{\partial^2 T}{\partial x^2} + \frac{\partial^2 T}{\partial y^2} = 0 \tag{2a}$$

$$-k_f \frac{\partial^2 T_f}{\partial x^2} + \rho U C_p \frac{\partial T_f}{\partial x} + \frac{2h(x)(b+e)}{b \cdot e}(T_f - T_p) = 0 \tag{2b}$$

$$\frac{\partial T}{\partial x} = 0 \qquad 0 \leqslant y \leqslant b, x = 0, x = L \tag{2c}$$

$$-k_s \frac{\partial T}{\partial y} = q \quad 0 \leqslant x \leqslant L, y = b \tag{2d}$$

$$-k_s \frac{\partial T}{\partial y} = h(x) \cdot (T_f - T_p) \quad 0 \leqslant x \leqslant L, y = 0 \tag{2e}$$

$$T_f = T_{in}, T_f = T_{out} \qquad x = 0, x = L \tag{2f}$$

The mathematical models obtained for each part of the field are discretized using the finite volume method. Numerical resolution of the problem for the solid part is achieved by the semi-iterative method line by line; numerical resolution of the problem in the fluid part is achieved by the direct Thomas algorithm. During resolution, the temperature at the volume interfaces in the convective term is obtained by a power law scheme. The algorithm used for the resolution of the coupled problem is iterative. After initialization, the problems in the solid zone and in the fluid zone are solved successively. For one problem, the temperature field of the other is considered known starting either from the initial choice for the first iteration or from the preceding iteration. Thus at each iteration, in the resolution of one of the problems, the temperatures calculated at the preceding step are reinjected in the computations

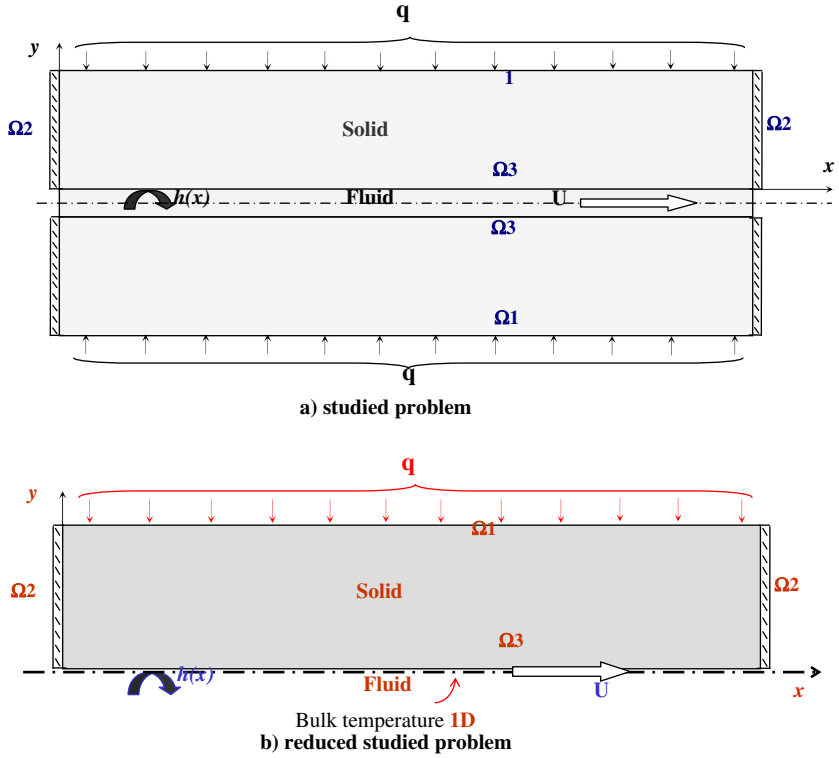

Fig. 6. Schematic representation problem.

until the least-squares convergence criterion (3) (the square root of the sum of the square of the differences in temperatures between two successive iterations) is satisfied:

$$\sqrt{\sum_i (T_f(i) - T_f^*(i))^2 + \sum_{ij} (T(i,j) - T^*(i,j))^2} < 10^{-6} \quad (3)$$

Resolution of the direct-coupled problem thus requires knowledge of the convective heat transfer coefficient along the channel. This formulation is adopted to allow determination of the evolution of this coefficient in the resolution of the inverse problem, since it is the principal unknown factor in this problem.

The use of conventional correlations for macrochannels [26] (Shah and London, 1978) to describe the convective heat transfer coefficient in the microchannel reveals the formation of a kind of macroconstriction in the walls that is translated by deformation of the constant heat flux iso-contour lines and the iso-temperature lines, as shown in Fig. 7a and b. These deformations clearly result from the fact that the heat flux follows a privileged direction in crossing the wall: towards the channel inlet because of the larger convective heat transfer coefficient at the microchannel entrance, which makes the thermal resistance a minimum in this direction. Therefore, at least a two-dimensional model must be used to estimate the wall temperature and the convective heat transfer coefficient, especially for low-Reynolds-number flows.

3.2. Sensitivity analysis and instrumentation of the microchannel

Resolution of the sensitivity problem is essential to the construction of the inverse problem, and also is also useful in devising instrumentation adequately sensitive to the variations of the estimated parameters. The sensitivity of measurement is defined as the derivative of the measured parameter with respect to the estimated parameter. The required parameters are the two coefficients present in expression (1) for $h(x)$. The measurement sensitivities of the estimated parameters are obtained by deriving the temperatures in each field with respect to the two coefficients C and h_∞, called S_h and S_c in the solid and S_h^f and S_c^f in the fluid. The derivation of the direct problem with the two parameters C and h_∞ led to Eqs. (4) and (5), which are solved by the same iterative procedure as the direct problem:

$$\frac{\partial^2 S_c}{\partial x^2} + \frac{\partial^2 S_c}{\partial y^2} = 0 \quad (4a)$$

$$-k_f \frac{\partial^2 S_c^f}{\partial x^2} + \rho U C_p \frac{\partial S_c^f}{\partial x} + \frac{(b+e)}{b \cdot e}\left[\frac{h_\infty}{x}(T_f - T_p) + h_\infty\left(1 + \frac{c}{x}\right)(S_c^f - S_c)\right] = 0 \quad (4b)$$

$$-k_s \frac{\partial S_c}{\partial x} = 0 \quad 0 \leqslant y \leqslant b, x = 0, x = L, 0 \leqslant x \leqslant L \quad (4c)$$

$$-k_s \frac{\partial S_c}{\partial y} = \frac{h_\infty}{x}(T_f - T_p) + h_\infty\left(1 + \frac{C}{x}\right)(S_c^f - S_c) \quad 0 \leqslant x \leqslant L, y = 0 \quad (4d)$$

$$S_c^f = 0 \quad x = 0, x = L \quad (4e)$$

$$\frac{\partial^2 S_h}{\partial x^2} + \frac{\partial^2 S_h}{\partial y^2} = 0 \quad (5a)$$

$$-k \frac{\partial^2 S_h^f}{\partial x^2} + \rho U C_p \frac{\partial S_h^f}{\partial x} + \frac{(b+e)}{b \cdot e}\left[\left(1 + \frac{c}{x}\right) h_\infty \left(S_h^f - S_h\right) + (T_f - T_p)\right] = 0 \quad (5b)$$

$$-k_s \frac{\partial S_h}{\partial x} = 0 \quad 0 \leqslant y \leqslant b, x = 0, x = L, 0 \leqslant x \leqslant L \quad (5c)$$

$$-k_s \frac{\partial S_h}{\partial y} = \left(1 + \frac{C}{x}\right)(T_f - T_p) + h_\infty\left(1 + \frac{C}{x}\right)(S_h^f - S_h) \quad 0 \leqslant x \leqslant L, y = 0 \quad (5d)$$

$$S_h^f = 0 \quad x = 0, x = L \quad (5e)$$

The explicit presence of the temperature in the two previous systems of equations requires knowledge of the temperature distribution to resolve the sensitivity problems. Hence, the direct

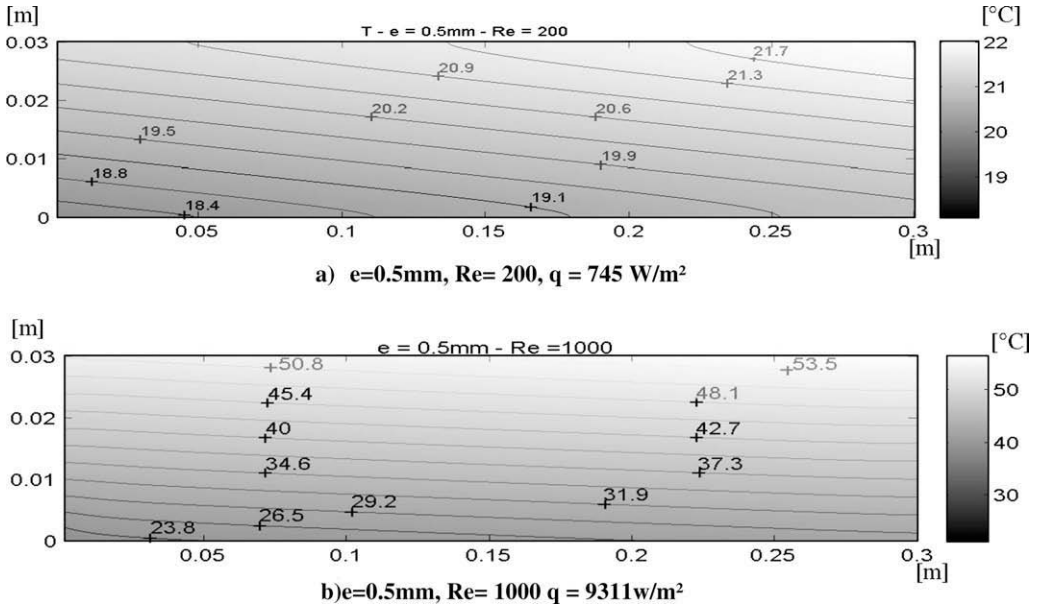

Fig. 7. Temperature distribution in solid wall along microchannel length.

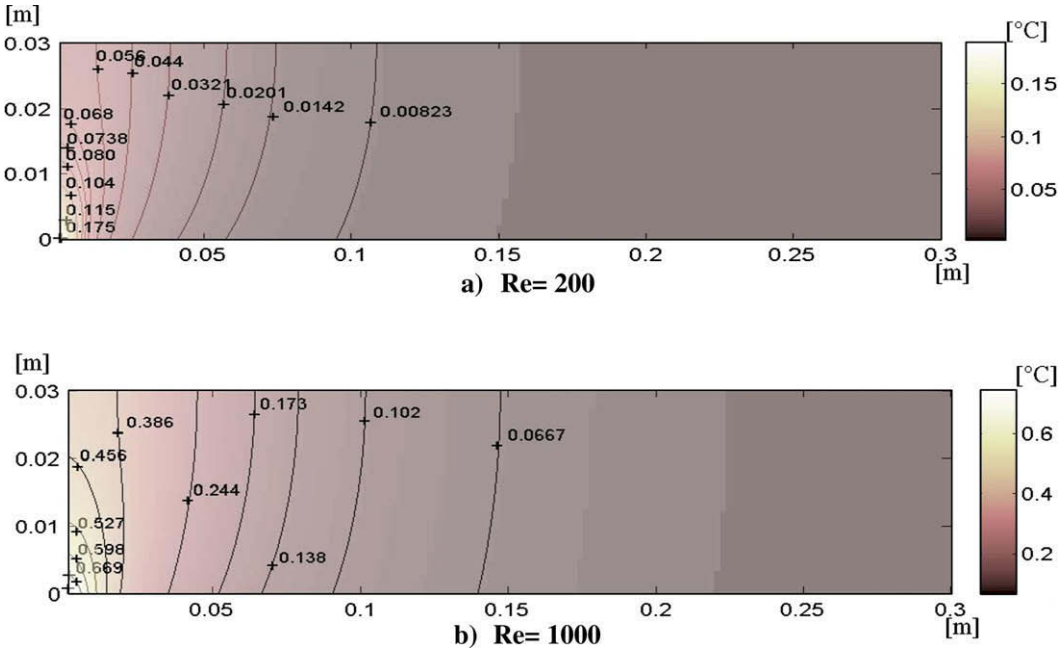

Fig. 8. Iso-sensitivity lines ($S_c^* C$) in half of the wall.

problem must be solved before the sensitivity problems. The resolution of the two systems allows determination of the sensitivity fields for the two parameters (h_∞ and C) in the walls.

Fig. 8a and b show the sensitivity of the parameter C expressed in [°C] (by multiplying the sensitivity S_c by the parameter C) for Reynolds numbers $Re = 200$ and 1000 and channel height 0.5 mm. The results reveal the importance of the parameter C in the channel entry, which is due to its role in the expression for $h(x)$. The value of parameter C determines the thermal entry length. For the two Reynolds numbers presented here, the flow is thermally developed more quickly for the first Reynolds number (200) than for the second (1000), which implies a higher sensitivity S_c for the fastest flow. Nevertheless, the measurement sensitivity S_c remains better in the channel entry and decreases along the channel for all flow regimes.

Iso-sensitivity lines for the parameter h_∞ expressed in [°C] (by multiplying the sensitivity S_h by the parameter h_∞) are plotted in Fig. 9a and b for the same Reynolds numbers. Analysis of the sensitivity S_h shows that the influence of h_∞ increases along the channel and in the wall vicinity. This behaviour of S_h can be explained by the fact that h_∞ represents the asymptotic value of the convective heat transfer coefficient in the thermally fully developed zone, which is thus prevalent at the channel exit.

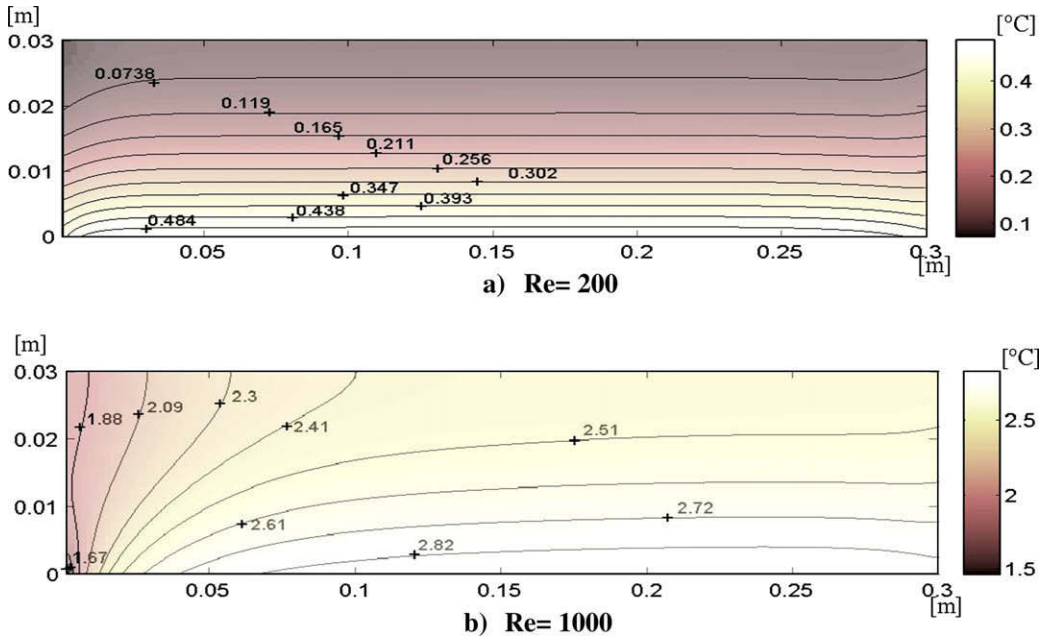

Fig. 9. Iso-sensitivity lines ($S_h^* h_\infty$) in the wall.

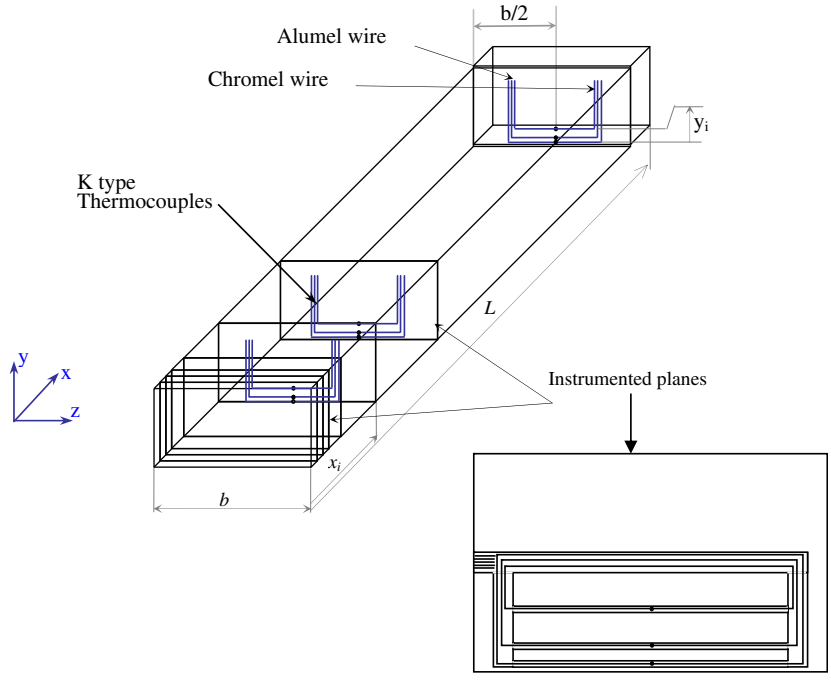

N° thermocouple	1	2	3	4	5	6	7	8
X [mm]	2	4	6	10	28	60	98	287
Y [mm]	0,459	0,420	0,489	0,275	0,278	0,496	0,360	0,407

Fig. 10. Position of thermocouples on upper block of microchannel and the thermocouples used in estimation.

3.3. Instrumentation of the microchannel by thermocouples

Estimation of the interface (solid–fluid surface) thermal conditions inside the microchannel requires use of an inverse method. Not only rigorous modelling of the heat transfers in the system but also knowledge of a certain number of temperatures in the walls thickness is needed. Indeed, these measured temperatures are used as input to the resolution of the inverse problem. Consequently, the quality of the estimate of the various parameters by the inverse method is directly related to the quality of the measurement of the input temperatures.

The position of the thermocouples is to be determined in the three directions x, y and z, as shown in Fig. 10. In the z direction, the thermocouples are positioned in the middle of the channel ($z = b/2$). This position in an isothermal zone is necessary for correct temperature measurement, as explained previously. Indeed, the temperature is uniform in this direction thanks to the precautions taken during design.

The sensitivity study in the last paragraph but one implies that the more sensitive zones must be instrumented more densely. Indeed, sensitivity to the parameter C is higher in the channel entry zone, whereas that to the parameter h_∞ is greater at the exit. The thermocouple instrumentation must cover all the channel length and must be refined in the most sensitive places, in particular in the channel entry where sensitivity of parameter C is high. In addition, the sensitivity of parameter h_∞ is almost constant in the x direction, after a few millimeters downstream of the channel entry. For technical reasons, the first instrumented plane is 2 mm from the microchannel entrance. The five other planes used to cover the developing zone are located at x-positions at which the convective conductance has varied 20% from its value at the previous position. Finally, two other instrumented planes are positioned at the exit of the channel so as to cover the fully developed zone.

Positioning of the thermocouples in the y direction is also guided by the sensitivity analysis, which revealed a higher measurement sensitivity closer to the interface. However, if the thermocouples are introduced too close to the interface, they can disturb heat conduction in the solid wall and modify the estimate of the wall surface temperature. The y position is a compromise between the sensitivity and the measurement accuracy. A good compromise suggested by Bourouga et al. (2000) [27] can be made by positioning the closest thermocouple at a distance ranging between 10 and 60 times the thermocouple bead diameter from the wall surface. The bead diameter of our thermocouples is 50 μm, so that the first thermocouple is implanted 500 μm from the wall surface. Two other thermocouples are placed at respective distances of 2.35 and 6.1 mm from the wall. All thermocouples need not be used to estimate the convective heat transfer coefficient. Indeed, only the most sensitive thermocouples, namely those at the entry and those nearest to the wall, are implanted in the inverse method. Many thermocouples were used here because of their fragility and possible breakdown during assembly of the microchannel and also during experimentation. Fig. 10 shows the longitudinal position of thermocouples and the y position of the thermocouples closest to the solid–fluid interface.

3.4. Inverse method for estimation of the convective heat transfer coefficient

The inverse method developed here uses the Gauss–Newton minimization algorithm. It consists in comparing temperatures measured experimentally and those estimated numerically at the same positions by imposing a given convective heat transfer coefficient. This estimate is obtained by minimization of the following least-squares function:

$$J(\delta^k) = \frac{1}{2}\sum_{i=1}^{N_t}[\tilde{T}_i(\delta^k) - T_i^*]^2 \tag{6}$$

where N_t is the thermocouple number, $\tilde{T}_i(\delta^k)$ are the temperatures computed numerically at iteration k and T_i^* the temperatures measured experimentally. The estimation algorithm can be summarized as follows:

1. Initial choice of the parameters $C = C^0$ and $h\infty = h_\infty^0$
2. Resolution of the direct problem: $\tilde{T}_i(\delta)$
3. Compute the least-squares function $J(\delta)$
4. Stop if the convergence criterion is satisfied ($J(\delta) \leqslant \varepsilon$) and take $C^* = C$, $h_\infty^* = h_\infty$; otherwise continue
5. Resolution of the sensitivity problems
6. Correct the parameters: $C = C + \Delta C$, $h_\infty = h_\infty + \Delta h$, where

$$\Delta\delta^k = [X^{kt} \cdot X^k]^{-1} X^{kt}[T_i^* - \tilde{T}_i] = [\Delta h, \Delta C] \tag{7}$$

7. Return to step 2

The algorithm starts with a vector δ^o corresponding to an arbitrary initial choice that has for coordinates the two parameters C^0 and h_∞^0 characterizing the convective heat transfer coefficient (1). At each iteration, the algorithm determines the vector δ^{k+1} that corrects the parameters to be estimated by minimizing the criterion J:

$$\delta^{k+1} = \delta^k + \Delta\delta^k \tag{8}$$

where

$$\Delta\delta^k = [X^{kt} \cdot X^k]^{-1} X^{kt}[T_i^* - \tilde{T}_i] \tag{9}$$

The correction $\Delta\delta^k$ brought to δ^k determines the modulus as well as the direction of the iterate displacement vector in the space $[C, h_\infty]$. Indeed, at each iteration the program corrects the displacement vector and approaches the target values.

In order to reduce the convergence time, some modifications have been made to the Gauss–Newton method that considerably reduces the number of iterations. Since the estimated parameters cannot be negative, the space $[C, h_\infty]$ is limited by excluding the negative values. In addition, the limits on the parameter values were chosen sufficiently high compared with the two variables h_∞ and C. This restricted space reduces the divergence of calculations by imposing a narrower search space.

In addition, the program can sometimes approach the target values without being able to reach them because of the size of the displacement vector δ^k. The modulus was optimized by introducing an under-relaxation that reduces the modulus of the displacement vector of reiterated $\Delta\delta^k$ by a coefficient μ^k, written as:

$$\mu^k = \frac{\alpha}{k} \cdot \left[\frac{J(\delta^k)}{J(\delta^0)}\right]^\beta \tag{10}$$

This coefficient is the ratio between the error obtained at iteration k and that at the first iteration that is the largest. Determination of the coefficients α and β in the expression for the relaxation coefficient (10) was done empirically. The values selected ($\alpha = 0.89$, $\beta = 0.55$) made it possible to reduce the number of iterations considerably.

4. Experimental results and discussions

4.1. Pressure losses

Pressure losses can be characterized by the Poiseuille number. For macrochannels, this number takes a constant value in the laminar regime depending only on the shape of the channel cross-section. On the other hand, when the flow becomes turbulent the Poiseuille number increases with the Reynolds number. In these experiments, the Poiseuille number can be estimated as well in the laminar regime as in the turbulent regime starting from the simultaneous measurement of the flow rate and the pressure drop between the entrance and the exit of the microchannel. The pressure drop is measured directly in the channel where the flow is hydrodynamically fully developed.

From the expressions for the friction coefficient and Reynolds number,

$$\mathrm{Re} = \frac{UD_h}{\nu} \tag{11}$$

$$f = \frac{\Delta P}{L}\frac{2D_h}{\rho U_2} \tag{12}$$

the value of the Poiseuille number can be obtained from:

$$P_0 = f \cdot Re = \frac{\Delta}{L}\frac{8e^2}{\rho \partial U} \tag{13}$$

The Poiseuille numbers is measured experimentally for all microchannel heights studied in the laminar and turbulent regimes. They are then compared in the laminar regime with the theoretical values given by (14) (suggested by Shah and London (1978) [26]), and the turbulent regime with the Blasius correlation (1913) [28] (15) and that of Kakaç et al. (1987) [29] (16):

$$P_0\mathrm{th} = 24[1 - 1.3553\alpha^* + 1.9467\alpha^{*2} - 1.7012\alpha^{*3} + 0.9564\alpha^{*4} - 0.2537\alpha^{*5}] \tag{14}$$

$$f = 0.0791Re^{-0.25} \quad \text{for :} \quad 5000 \le Re \le 3 \times 10^4 \tag{15}$$

$$f = (1.0875 - 0.1125\alpha^*)f_c \quad \text{for :} \quad 4 \times 10^3 \le Re \le 10^7 \tag{16}$$

where $f_c = 0.00128 + 0{,}1143\ Re^{-0.311}$ and $\alpha^* = e/b$, where e is the channel height and b its width.

Fig. 11a–d plot the evolution of the Poiseuille number against the Reynolds number for various microchannel heights. It can be seen that in the laminar regime, the values of the experimental

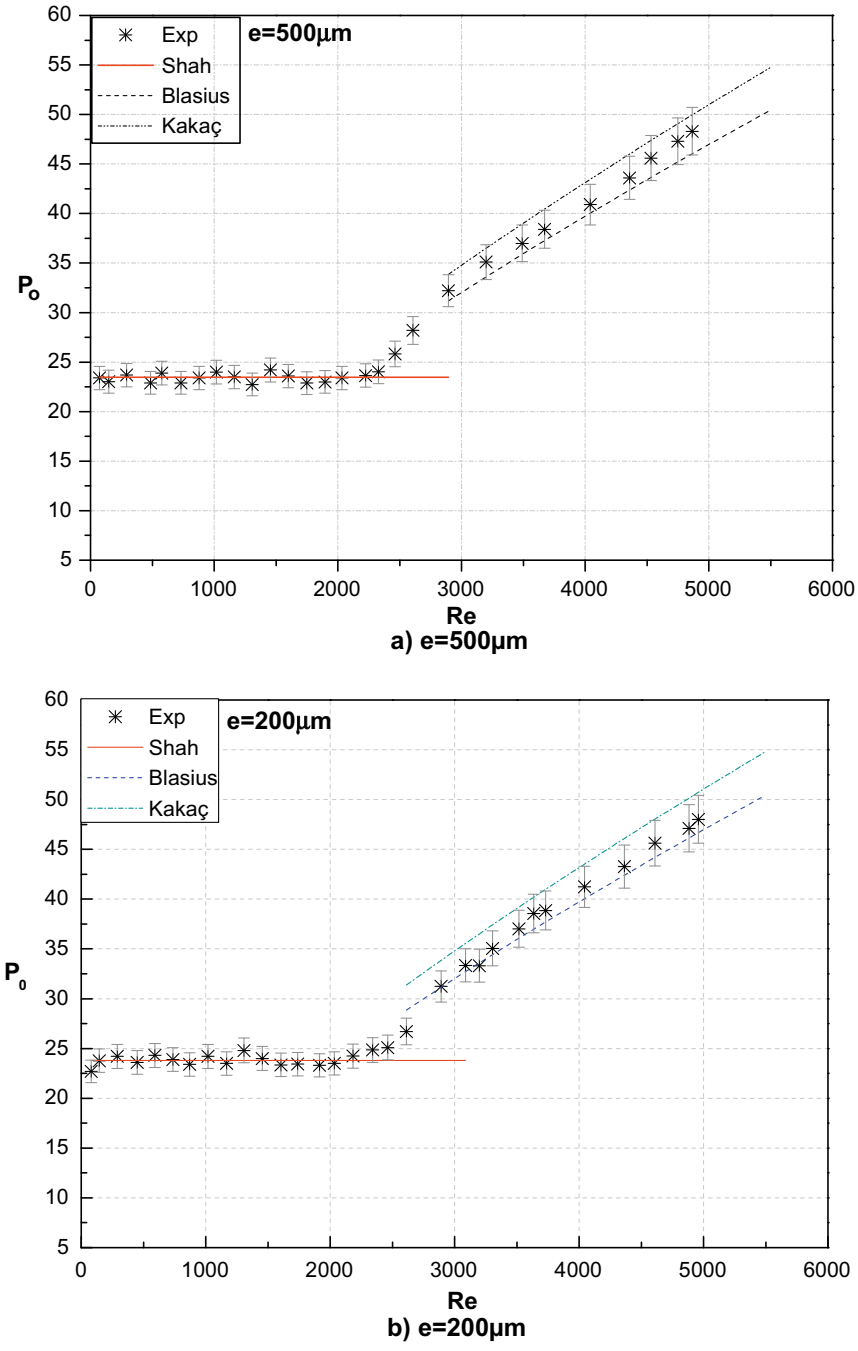

Fig. 11. Comparison of experimental Poiseuille number with classical correlations for various Reynolds numbers.

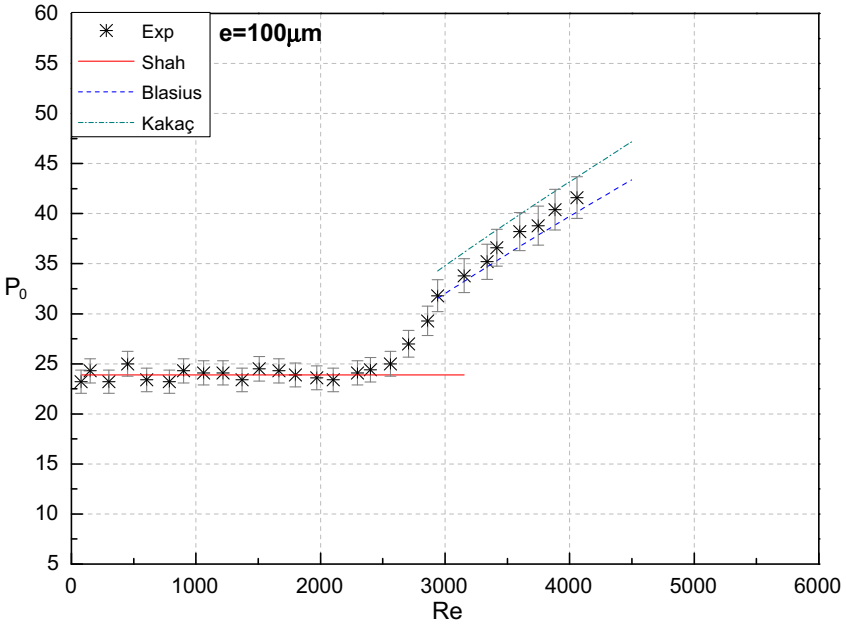

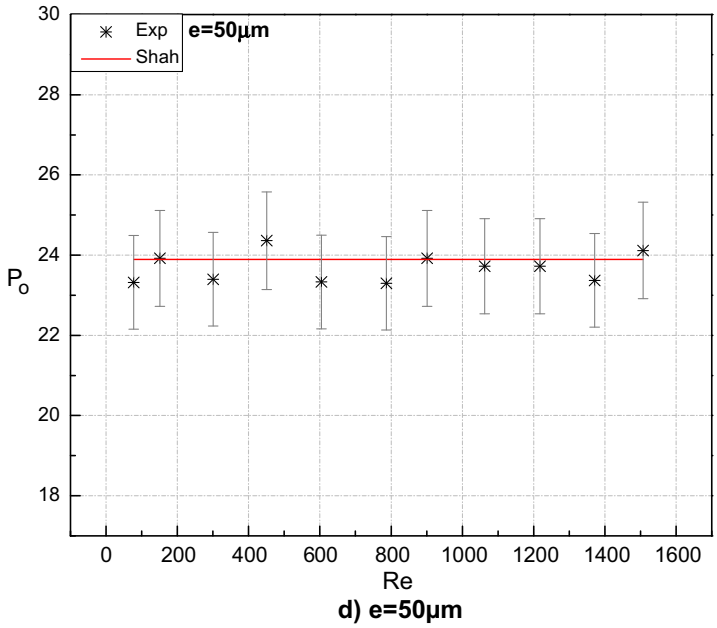

Fig. 11 (*continued*)

Poiseuille numbers are in good agreement with the theoretical values obtained from (14). In the turbulent regime, the pressure losses obtained in the Blasius expression are slightly lower than the experimental values, but the difference is smaller than the measurement uncertainties. It is noted in addition that the measurements lie between the Blasius [28] correlation obtained for ducts of rectangular cross-section with large aspect ratio and the one recommended by Kakaç et al. [29] for rectangular ducts.

In addition, the experimental results obtained for microchannel heights ranging between 500 and 100 µm show that the transition Reynolds number is clearly located between 2000 and 3000.

4.2. Nusselt number

The convective heat transfer in the microchannel flow is characterized by two Nusselt numbers. The first, denoted Nu_H and defined in the thermally and hydrodynamically fully developed zone, is given directly by the parameter estimation program. Its value is constant in the laminar regime and depends only on the shape of the duct cross-section and the wall thermal conditions. The second Nusselt number, denoted Nu_m, characterizes the mean convective heat transfer in the microchannel; its value is defined by:

$$Nu_m = \frac{1}{L}\int_0^L Nu(x)\mathrm{d}x \tag{17}$$

The value of this average Nusselt number includes the convective heat transfers in the developing and fully developed zones. Its experimental value is compared in the laminar regime with the theoretical value given by the Shah and London correlations [26]; in the turbulent regime it is compared with the values given by the Gnielinski (1976) [30] and Dittus and Boelter (1985) [31] correlations.

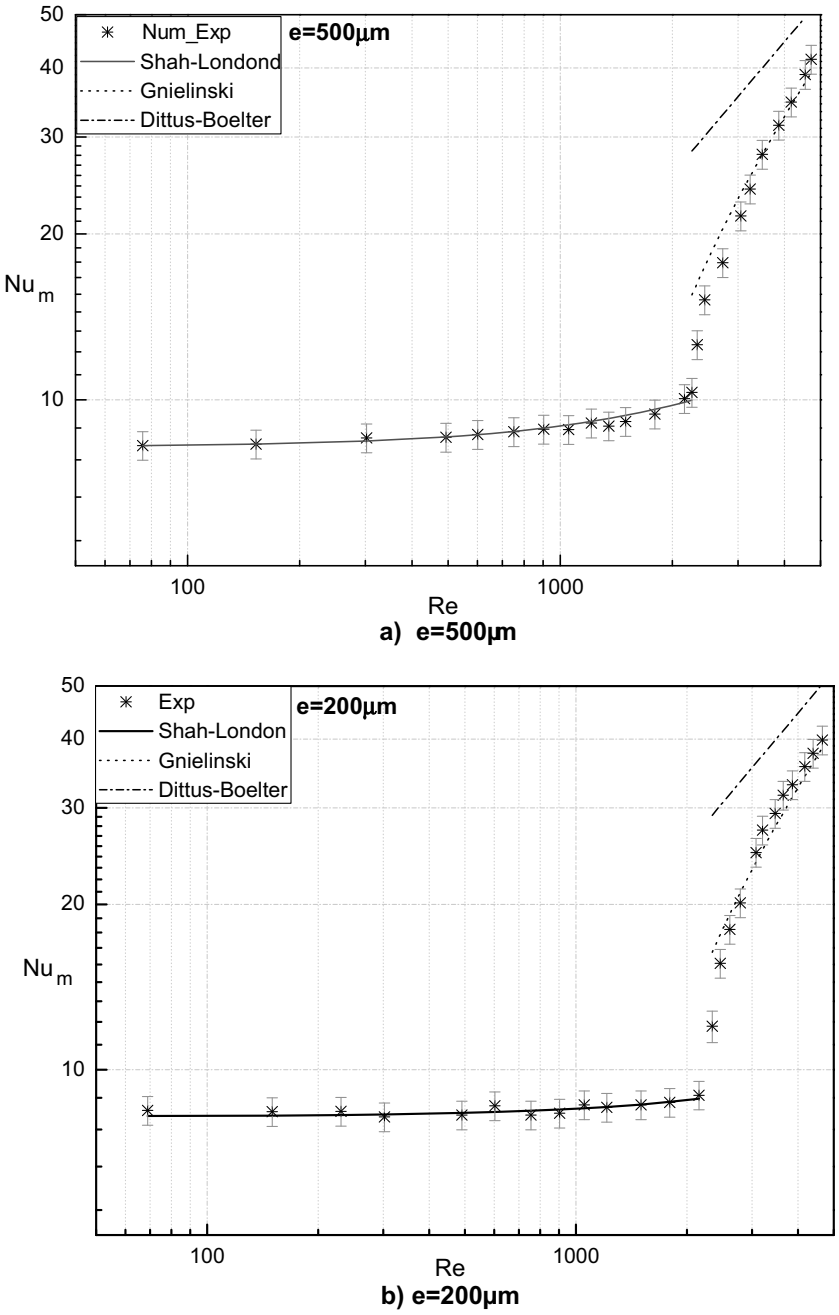

Fig. 12. Comparison of the experimental Nusselt number with classical correlations for various Reynolds numbers.

The experimental results and theoretical values for Nu_m as a function of Reynolds number flow are compared in Fig. 12a–d for all microchannel heights studied here. They show that the experimental average Nusselt numbers obtained in the laminar regime are in very good agreement with the values given by the Shah and London correlations [26]. In addition, the average Nusselt number value increases slightly with increasing Reynolds number in the laminar regime. This Nusselt number behavior has been presented in some studies [8,32,33] as new, but it is in fact the normal behavior of the average Nusselt number for flows in the entry zone of thermally developing channel flows.

The increase in the average or total Nusselt number is clearly explained by the fact that in the thermal developing length the flow is still Reynolds-number-dependent. This tendency continues in the turbulent regime, where the development length decreases with increasing Reynolds number. Values of the average Nusselt numbers obtained experimentally in the turbulent regime are in good agreement with those given by the Gnielinski correlations [30]. The results presented in Fig. 12a–d for channel heights between 500 and 100 µm reveal that the transition between laminar and turbulent regimes occurs at Reynolds numbers ranging between approximately 2200 and 3000.

Finally, experiments with channel height 50 µm did not allow exploration of the transition zone or the turbulent regime due to pump capacity limitations. Nevertheless, the results plotted in Fig. 12d in the laminar regime are in good agreement with Shah and London's correlations [26].

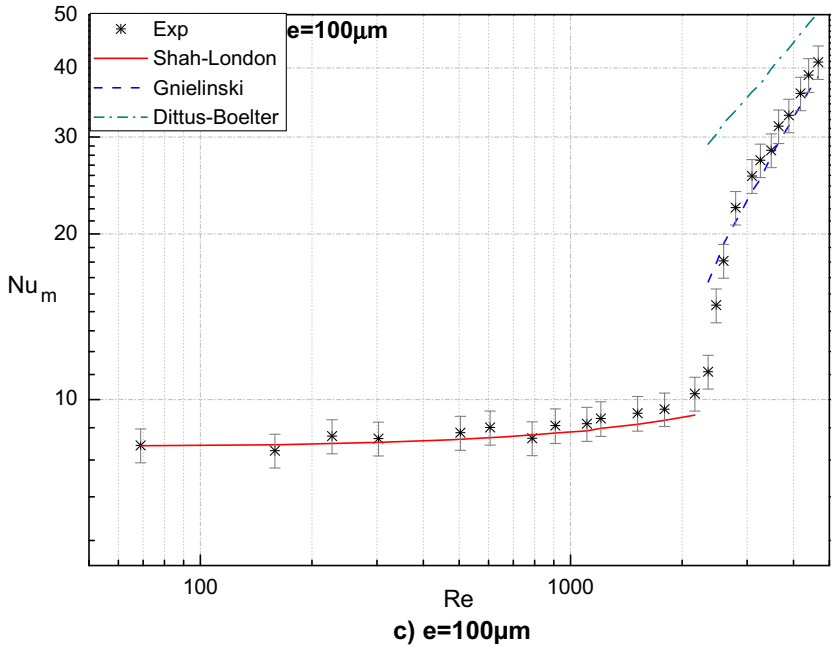

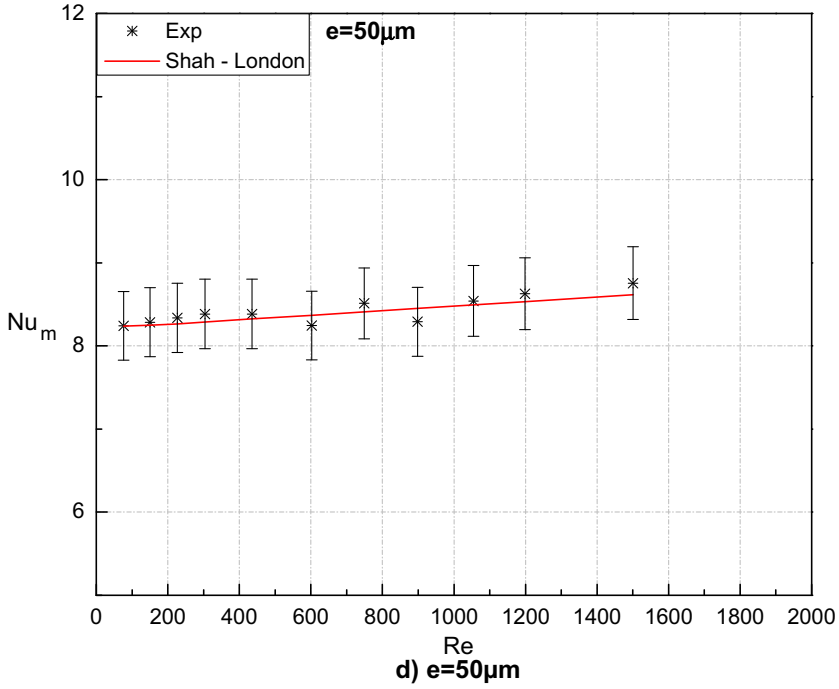

Fig. 12 (*continued*)

The influence of the hydraulic diameter can be observed thanks to the representation of the Nusselt number versus the Cameron number $X^*(X^* = \frac{x/D_h}{Re.Pr})$. If the microchannel's size has no influence, all the values of the local Nusselt numbers should collapse to only one curve. The evolution of the Nusselt number for Reynolds number 150 for all the thicknesses studied is represented in Fig. 13. The Nusselt number values are clearly superimposed and contained in an interval of approximately 5%, which corresponds, in fact, to the estimated uncertainty for the convective heat transfer coefficient in the fully developed zone. The local Nusselt number is not sensitive to reduction of the hydraulic diameter. However, the 5% interval in which the curves in Fig. 13 are contained is explained by the fact that at this Reynolds number the flows are relatively quick to attain a fully developed state. The value of the fully developed Nusselt number has a prevailing role along the channel in the local value of the Nusselt number.

4.3. Discussion

Recent measurements of pressure losses carried out inside the ducts (Khol et al. [34] and Bavière et al. [35]) also found good agreement with the correlations conventionally used in the fluid dynamics. Meinhart et al. [36] also confirmed these results by local velocity measurements with PIV.

The two studies estimating the wall temperature indirectly via a one-dimensional model are the recent work of Lelea et al. [14] and

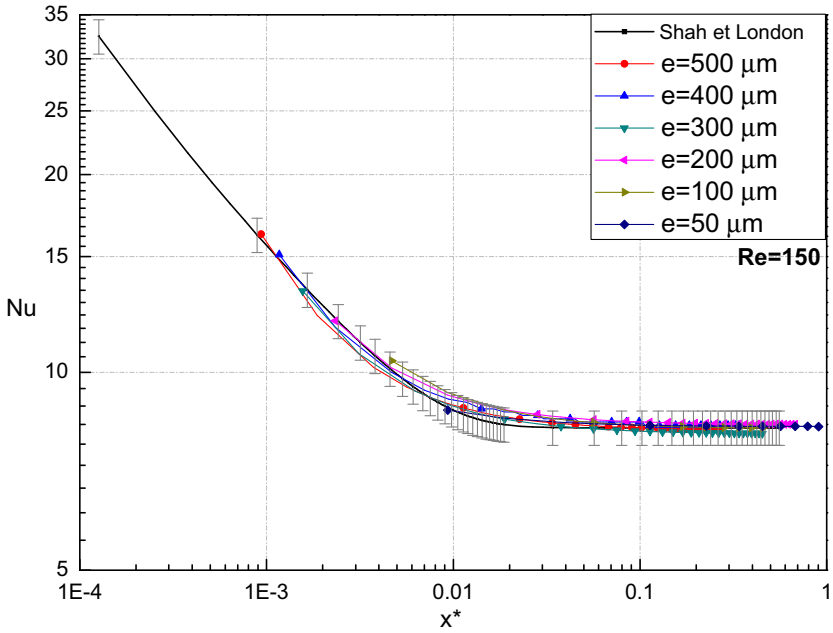

Fig. 13. Comparison of the experimental local Nusselt number with classical correlations for all studied thicknesses (Re = 150).

Lee et al. [15]. By taking into account the developing zones, these authors made local measurements of the convective heat transfer coefficient along the ducts. The results obtained by the latter are suitably described by the conventional correlations.

It seems that measurement errors as well as entrance-zone phenomena are the cause of the dispersions in the results and their deviation from the macro-size channel correlations noted in many studies of the flow and convective heat transfer in microchannels. Indeed, from the hydrodynamic point of view all these studies have shown deviations from the theory, where the pressure losses were measured in mini-feed basins outside the ducts. This type of measurement includes on the one hand the singular pressure losses due to the connections, and on the other the pressure losses generated by the hydrodynamic flow development. These two pressure losses are obviously not constant for the same duct since they depend on the flow rate in addition to duct geometry. The two pressure losses are added to the regular pressure losses used to determine the friction coefficient or the Poiseuille number and hence contribute to their overestimation.

However, this description does not explain the reductions in pressure losses reported in the literature. Another parameter that can explain the dispersion of the results in the literature is probably the hydraulic diameter of the tested ducts. Its influence is indeed considerable, since it appears with power 4 in the expressions for the Poiseuille number.

From the heat transfer point of view, in many studies the wall temperatures at the fluid-solid interface were measured on the outer face of the walls. Since one of the common characteristics of microchannels is their relatively high wall thickness, this type of measurement can cause significant errors in the convective heat transfer coefficients. Moreover, the heating zones in many experimental devices are often not precisely controlled. Studies are frequently carried out in flows in a thermally and hydrodynamically developing state, while the results are then compared with the correlations or theoretical values valid for fully developed flows. In some experiments in the literature the thermocouples are directly fixed to the fluid-solid interface. This type of measurement clearly gives access to the average temperature between the fluid and the solid wall, not to the actual wall temperature.

5. Conclusions

The main conclusion of this study is that the conventional laws and correlations describing the flow and convective heat transfer in ducts of large dimension are directly applicable to the microchannels of heights between 500 and 50 microns. In addition, we showed that the transition from the laminar to turbulent regime occurred in a range of Reynolds numbers similar to that observed in ducts of large sizes.

References

[1] S.B. Choi, R.F. Barron, R.O. Warrington, Fluid flow and heat transfer in microtubes, in: Micromechanical Sensors, Actuators and Systems, vol. 32, ASME DSC, Atlanta, GA, 1991, pp. 123–134.
[2] M. M. Rahman, F.J. Gui, Experimental measurements of fluid flow and heat transfer in microchannel cooling passages in a chip substrate, advances in electronic packaging, in: ASME EEP, vol. 199 (1993), pp. 685–692.
[3] D. Yu, R.O. Warrington, R. Barron, T. Ameel, An experimental and theoretical investigation of fluid flow and heat transfer in microtubes, Proceedings of ASME/JSME Thermal Engineering Joint Conf, Maui, HI, 1995, pp. 523–530.
[4] J.M. Cuta, C.E. McDonald, A. Shekarriz, Forced convection heat transfer in parallel channel array microchannel heat exchanger, in: Advances in Energy Efficiency, Heat/Mass Transfer Enhancement, in: ASME-PID, 2/HTD, vol. 338, 1996, pp. 17–23.
[5] T.M. Adams, S.I. Abdel-Khalik, S.M. Jeter, Z.H. Qureshi, An experimental investigation of single-phase forced convection in microchannels, Int. J. Heat Mass Transfer 41 (1998) 851–857.
[6] M.M. Rahman, Measurements of heat transfer in microchannel heat sinks, Int. Commun. Heat Mass Transfer 27 (2000) 495–506.
[7] X.F. Peng, B.X. Wang, Forced convection and flow boiling heat transfer for liquid flowing through microchannels, Int. J. Heat Mass Transfer 36 (1993) 3421–3427.
[8] B.X. Wang, X.F. Peng, Experimental investigation on liquid forced convection heat transfer through microchannels, Int. J. Heat Mass Transfer Suppl. 37 (1) (1994) 73–82.
[9] C.P. Tso, S.P. Mahulikar, Experimental verification of the role of Brinkman number in microchannels using local parameters, Int. J. Heat Mass Transfer 43 (2000) 1837–1849.
[10] W. Qu, G.M. Mala, D. Li, Heat transfer for water flow in trapezoidal silicon microchannels, Int. J. Heat Mass Transfer 43 (2000) 3925–3936.
[11] F. Debray, J.P. Franc, T. Maitre, S. Reynaud, Mesure des coefficient de transfert thermique par convection forcée en mini-canaux, Mec. Ind. 2 (2001) 443–454.
[12] P. Gao, S. Le Person, M. Favre-Marinet, Scale effects on hydrodynamics and heat transfer in two-dimensional mini and microchannels, Int. J. Therm. Sci. 41 (2002) 1017–1027.

[13] W. Qu, I. Mudawar, Experimental and numerical study of pressure drop and heat transfer in a single-phase micro-channel heat sink, Int. J. Heat Mass Transfer 45 (2002) 2549–2565.
[14] D. Lelea, S. Nishio, K. Takano, Experimental research on microtube heat transfer and fluid flow of distilled water, Int. J. Heat Mass Transfer 47 (2004) 2817–2830.
[15] P.S. Lee, S.V. Garimella, D. Liu, Investigation of heat transfer in rectangular microchannels, Int. J. Heat Mass Transfer 48 (2005) 1688–1704.
[16] J. Pfahler, J. Harley, H.H. Bau, J.N. Zemel, Gas and liquid flow in small channels, Micromechanical Sensors, Actuators and Systems, ASME DSC 32, Atlanta, GA, 1991, pp. 49–60.
[17] G.M. Mala, D. Li, Flow characteristics of water in microtubes, Int. J. Heat Fluid Flow 20 (1999) 142–148.
[18] C.L. Merkle, T. Kubota, D.R.S. Ko, An analytical study of the effects of surface roughness on boundary-layer transition, AFOSR Space and Missile Sys Org., AD/A004786.3, 1974.
[19] I. Tani, Boundary-layer transition, Annual Reviews of Fluid Mechanics, I, Annual Reviews, Tioga, Palo Alto, CA, 1969.
[20] G.M. Mala, D. Li, J.D. Dale, Heat transfer and fluid flow in microchannels, Int. J. Heat Mass Transfer 40 (1997) 3079–3088.
[21] S. Colin, Microfluidique, Hermes Science Publications, 2004.
[22] X.F. Peng, G.P. Peterson, B.X. Wang, Frictional flow characteristics of water flowing through rectangular microchannels, J. Exp. Heat Transfer 7 (1995) 249–264.
[23] M.H. Sabry, Scale effects on fluid flow and heat transfer in microchannels, IEEE Trans. Compon. Pack. Technol. 23 (3) (2000) 562–567.
[24] Z.-Y. Guo, Z.-X. Li, Size effect on microscale single-phase flow and heat transfer, Int. J. Heat Mass Transfer 46 (2003) 149–159.
[25] G. Hetsroni, A. Mosyak, E. Pogrebnyak, L.P. Yarin, Fluid flow in micro-channels, Int. J. Heat Mass Transfer 48 (2005) 1982–1998.
[26] R.K. Shah, A.L. London, Laminar Flow Forced Convection in Ducts, Academic Press, 1978.
[27] B. Bourouga, V. Goizet, J-P Bardon, Les aspects théoriques régissant l'instrumentation d'un capteur thermique pariétal à faible inertie, Int. J. Therm. Sci 39 (2000) 96–109.
[28] H. Blasius, Das Ähnlichkeitsgesetz bei Reibungvorgängen in Flüssigkeiten, Forchg. Arb. Ing.-Wes., 131, Berlin, 1913.
[29] S. Kakaç, R.K. Shah, W. Aung, Handbook of Single-Phase Convective Heat Transfer, Wiley-Interscience, 1987.
[30] V. Gnielinski, New equations for heat and mass transfer in turbulent pipe and channel flow, Int. Chem. Eng. 16 (1976) 359–368.
[31] P.W. Dittus, L.M.K. Boelter, Heat transfer in automobile radiators of tubular pipe, Int. Commun. Heat Mass Transfer 12 (1985) 3–22.
[32] X.F. Peng, B.X. Wang, G.P. Peterson, H.B. Ma, Experimental investigation of heat transfer in flat plates with rectangular microchannels, Int. J. Heat Mass Transfer 38 (1995) 127–137.
[33] H.Y. Wu, P. Cheng, An experimental study of convective heat transfer in silicon microchannels with different surface conditions, Int. J. Heat Mass Transfer 46 (2003) 2547–2556.
[34] M.J. Kohl, S.I. Abdel-Khalik, S.M. Jeter, S.D. Sadowski, A microfluidic experimental platform with internal pressure measurements, Sensor Actuators A 118 (2005) 212–221.
[35] R. Bavière, F. Ayela, Mesures locales de pertes de charge dans des microcanaux à l'aide de transducteurs micro-usinés, 2ème Congrès Français de Microfluidique, 2004, pp. 14–16.
[36] C.D. Meinhart, S.T. Wereley, J.G. Santiago, PIV measurements of a microchannel flow, Exp. Fluids 27 (1999) 414–419.
[37] J. Judy, D. Maynes, B.W. Webb, Characterization on frictional pressure drop for liquid flows through micro-channels, Int. J. Heat Mass Transfer 45 (2002) 3477–3489.
[38] D. Pfund, D. Rector, A. Shekarriz, A. Popescu, J. Welty, Pressure drop measurements in a microchannel, AIChE J. 46 (2000) 1496–1507.
[39] I. Papautsky, J. Brazzle, T. Ameel, A.B. Frazier, Laminar fluid behaviour in microchannels using micropolar fluid theory, Sensors Actuator A73 (1999) 101–108.
[40] J. Pfalher, J. Hardey, H.H. Bau, J.N. Zemel, Gas, liquid transport in micron and submicron channels, Sensors Actuators A 21–23 (1990) 431–434.
[41] P. Wilding, J. Pfalher, J.N. Zemel, H.H. Bau, L.J. Kricka, Manipulation and flow of biological fluids in straight channels micromachined in silicon, Clin. Chem. 40 (1994) 43–47.
[42] X.N. Jiang, Z.Y. Zhou, J. Yao, Y. Li, X.Y. Ye, Micro-fluid flow in microchannel, Proceeding of Transducers '95, 1995, pp. 317–320.
[43] S.M. Flockart, R.S. Dhariwal, Experimental and numerical investigation into the flow characteristics of channels etched in <100> silicon, J. Fluid Eng. 120 (1998) 291–295.